coatings

MDPI

Communication

Promoting the Segregation of Sr^{2+} from the Perovskite Oxygen Catalyst $La_{0.5}Sr_{0.5}Co_{3-\delta}$ via Quenching

Fa Zheng [1,2], Yaozheng Qian [2] and Shengli Pang [2,*]

[1] R&D Department, Jiangsu Yushi Energy Group Co., Ltd., Nantong 226500, China
[2] Institute for Advanced Materials, School of Materials Science and Engineering, Jiangsu University, Zhenjiang 212013, China
* Correspondence: slpang@ujs.edu.cn

Abstract: The microstructure of the surface plays a crucial role in determining the efficacy of high-temperature oxygen catalysts. In this study, we conducted a comprehensive investigation into the impact of quenching on the crystal structure, surface topology, and oxygen-catalyzing capabilities of $La_{0.5}Sr_{0.5}CoO_{3-\delta}$ (LSC). Our findings revealed that quenching can notably promote the segregation of SrO on the surface of the classical perovskite-based high-temperature oxygen catalyst LSC. This phenomenon can be attributed to the introduction of a significant number of chemical defects within the LSC bulk during the catalytic process, thereby endowing it with sufficient stress and electrostatic forces to drive Sr^{2+} toward the catalyst's surface. This finding could simplify the removal of inert segregation layers on the surface of perovskite-based high-temperature oxygen catalysts. The electrochemical analysis results demonstrate that the quenching process can markedly improve the long-term operational stability of LSC but can bring a decrease in catalytic activity.

Keywords: solid oxide fuel cells; oxygen electrocatalyst; segregation layers; quenching; perovskite oxide

check for updates

Citation: Zheng, F.; Qian, Y.; Pang, S. Promoting the Segregation of Sr^{2+} from the Perovskite Oxygen Catalyst $La_{0.5}Sr_{0.5}Co_{3-\delta}$ via Quenching. *Coatings* **2023**, *13*, 2032. https://doi.org/10.3390/coatings13122032

Academic Editor: Ioannis V. Yentekakis

Received: 9 November 2023
Revised: 28 November 2023
Accepted: 29 November 2023
Published: 30 November 2023

Copyright: © 2023 by the authors. Licensee MDPI, Basel, Switzerland. This article is an open access article distributed under the terms and conditions of the Creative Commons Attribution (CC BY) license (https://creativecommons.org/licenses/by/4.0/).

1. Introduction

Solid oxide fuel cells (SOFCs) are a green power source capable of efficiently generating electricity using hydrogen, natural gas, and biomass fuels [1–3]. The application of this technology is instrumental in addressing the increasingly pressing environmental and energy challenges. Similar to other battery structures, SOFCs consist of three components: the cathode, anode, and electrolyte. High cathodic polarization resistance, related to the sluggish oxygen reduction reaction process, stands as a critical factor limiting the electrochemical performance of SOFCs. Therefore, developing catalysts for oxygen reduction reactions with high catalytic activity and operational durability is of paramount importance in advancing SOFCs.

Perovskite structure metal oxides and their derivatives are among the most researched cathode catalysts for SOFCs [4–9]. Their general formula can be represented as ABO_3 and A_2BO_4, where the A-site is primarily composed of lanthanides and/or alkali earth metals, and the B-site consists mainly of transition metal elements. Perovskite structure catalysts and their derivative materials offer a wide range of choices for elements at both the A and B sites, with a substantial presence of chemical defects and lattice strains, providing a rich reaction environment for oxygen reduction behavior [10,11]. Over the past few decades, numerous perovskite-based oxides have been used as cathode catalysts, but few have met the catalytic activity and operational durability requirements of SOFCs. This is primarily due to the high-temperature nature of SOFCs, with a typical operating temperature range of 500–800 °C. At such elevated temperatures, the metal cations within perovskite catalysts possess high kinetic energy, and under the combined influence of lattice strain and electrostatic forces arising from chemical defects, certain alkali earth metals tend to segregate on the catalyst's surface, forming electrochemically inert coatings [12–23]. Cao

et al. discovered that $La_{0.6}Sr_{0.4}CoO_{3-\delta}$ exhibits Sr segregation on its surface at 600 °C, and prolonged exposure at this temperature for 72 h results in a more than two orders of magnitude increase in polarization resistance [12]. Feng et al. confirmed that high temperature is a key parameter leading to Sr segregation [22]. We found that due to Ba ion segregation on the surface and the formation of corresponding inert coatings, $PrBaCoCuO_{5+\delta}$ experiences a degradation rate as high as 17.8% per 100 h when operating at 700 °C [13]. The surface segregation of alkaline earth elements on perovskite-based high-temperature oxygen catalysts is a critical factor limiting their application in the field of SOFCs.

In response to the issue of alkali earth element segregation on perovskite-based oxygen catalysts at SOFCs' operating temperatures, numerous solutions have been proposed [12,17,24–37]. For example, Cao et al. discovered that acid treatment can effectively remove the inert coatings on the surface of $La_{0.6}Sr_{0.4}CoO_{3-\delta}$, thereby restoring the catalytic activity of the deteriorated catalyst [12]. Lee et al. found that only ~0.8% tensile strain can significantly reduce the Sr surface segregation of $La_{0.6}Sr_{0.4}CoO_{3-\delta}$ and increase its catalytic activity for oxygen reduction reactions by two orders of magnitude [36]. Zhuang et al. found that the reversible capture of segregating Sr on the surface of $(La_{0.6}Sr_{0.4})_{0.95}Co_{0.2}Fe_{0.8}O_{3-\delta}$ keeps the surface clean and highly active [38]. Li et al. found that the in situ introduction of SrO on the surface of $La_{0.6}Sr_{0.4}CoO_{3-\delta}$ induces the formation of highly electrochemically active reaction sites from the segregating Sr [24]. In our previous work, we found that the spontaneous reaggregation of segregated Ba and Fe elements on the surface of $Nd_{1/2}Ba_{1/2}Co_{1/3}Fe_{1/3}Mn_{1/3}O_{3-\delta}$ effectively avoids blocking the active sites on the surface [25]. Surface coating is a commonly used surface modification method in the field of new energy [34]. However, the complexity of the preparation process for nanoscale inert coating layers on perovskite catalyst surfaces and the associated high production costs severely limit their commercial application [33,34]. In fact, the compositional segregation of perovskite catalysts under SOFCs' working conditions fundamentally results from the imbalanced release of stress and electrostatic forces between ionic radius mismatches and chemical defects [26,39]. At room temperature, the interactions in such polycrystalline materials are locked within the lattice due to the low kinetic energy of metal cations. In the temperature range of 500–800 °C, the more vigorous vibrations of metal cations within the lattice, owing to their higher kinetic energy, push these locked interactions to drive the segregation of metal cations to the surface [12,24]. Previous research has mostly focused on how to suppress the segregation of alkaline earth metals. If a method can be found to promote alkaline earth metal segregation on the surface of catalyst particles, removing the segregation layer and then preparing the catalyst as a cathode, it is expected to effectively solve the problem of catalyst segregation.

In this study, we made a novel finding that quenching can promote the segregation of Sr^{2+} ions in the form of weakly crystalline SrO on the surface of $La_{0.5}Sr_{0.5}CoO_{3-\delta}$ (LSC). Compared to the cleaning of surface segregation layers, particularly post-operation, on SOFCs' cathodes, the treatment of SrO segregation layers on catalyst powder surfaces at room temperature becomes considerably simpler. This work holds the potential to open up a new approach for modifying SOFC cathode powders.

2. Materials and Methods

2.1. Materials

The preparation process for LSC-S and LSC-Q followed a procedure similar to our previously reported method [40]. In brief, the procedure involved weighing lanthanum nitrate, strontium nitrate, cobalt nitrate, citric acid, and ethylenediaminetetraacetic acid (EDTA) in accordance with the stoichiometric ratio, dissolving them in deionized water, and adjusting the pH to approximately 7 using ammonia solution. The molar ratio of metal cations, citric acid, and EDTA was 1:2:1. The metal salt solutions underwent sol–gel formation at 80 °C, carbonization at 250 °C, decarbonization at 600 °C, and phase transformation at 1000 °C to obtain the perovskite-structured oxygen catalyst LSC. The key

difference between LSC-Q and the reference sample LSC-S lies in the cooling process after the 1000 °C phase transformation for 4 h. LSC-S was slowly cooled in an air atmosphere at 0.05 °C s^{-1}, following traditional methods. In contrast, LSC-Q involved rapidly transferring the sample, after 4 h sintering at 1000 °C, into liquid nitrogen, resulting in an actual maximum cooling rate more than 8000 times higher than that of LSC-S (greater than 400 °C s^{-1}). To investigate the impact of sintering temperature during the cathode layer preparation process on LSC-S and LSC-Q, both materials were subsequently sintered at 900 °C in an air atmosphere for 4 h, separately.

2.2. Characterization

The phase structures of LSC-S, LSC-Q, and their annealed counterparts were analyzed using the X-ray diffraction (XRD) technique. The evolution of mass with temperature for LSC-S at room temperature was analyzed through the thermogravimetric analysis (TGA) technique. The surface chemical environments of annealed LSC-S and LSC-Q were examined using the X-ray photoelectron spectroscopy (XPS) technique. The microstructures of LSC-Q, the LSC-S annealed sample, and the LSC-Q annealed sample were observed with transmission electron microscopy (TEM) technique. The morphologies of the bulk LSC-S, LSC-Q, the LSC-S annealed sample, and the LSC-Q annealed sample cross-sections were analyzed using the scanning electron microscopy (SEM) technique. Additionally, SEM was also employed to analyze the morphology of the single-cell cross-section and the LSC-Q cathode after long-term discharge testing.

The fabrication of symmetric cells and single cells was documented in our previous work [40]. Notably, the electrolyte for the symmetric cells was $Ce_{0.9}Gd_{0.1}O_{1.95}$ (GDC). The single cells employed an anode-supported structure with NiO-YSZ/YSZ/GDC half-cell components, obtained from Ningbo SOFCMAN Energy Group Co., Ltd. Both LSC-S and LSC-Q cathodes were sintered at 900 °C for 4 h. The electrochemical impedance spectroscopy of symmetric cells was conducted at different temperatures in an air atmosphere using an electrochemical workstation (Solartron 1260 + 1287). The single cells were subjected to current–voltage–power density (I-V-P) curve measurements at 800 °C and 750 °C. Additionally, the power density evolution with time at 750 °C and 0.7V was monitored. The testing fuel consisted of pure hydrogen gas (99.99%), while the oxidant was flowing air. The testing system for SOFCs was established in our laboratory.

3. Results and Discussion

As detailed in the experimental section, there was a significant difference in the heat treatment process during the preparation of LSC-S and LSC-Q. LSC-S was obtained through slow cooling (0.05 °C s^{-1}) in air, and as shown in Figure 1a, it exhibits a cubic perovskite phase (icsd43178) at room temperature. On the other hand, LSC-Q was obtained by rapidly transferring LSC from 1000 °C to liquid nitrogen (approximately −200 °C). The estimated cooling rate was ~400 °C s^{-1}, roughly 8000 times that of LSC-S. Interestingly, LSC-Q still retains the perovskite phase structure (Figure 1a). Moreover, as shown in Figure 1b, the diffraction peaks of LSC-Q shifted towards lower angles by ~0.04° compared to LSC-S, indicating that the quenching process causes lattice expansion in LSC. We observed a similar phenomenon in our previous research [30], where quenched samples retained lower oxygen content at 1000 °C. Figure 1c illustrates that during heating in air, some oxygen in the perovskite lattice of LSC is released under the driving force of oxygen chemical potential. In the quenching process, LSC with a high temperature of 1000 °C is rapidly transferred to liquid nitrogen for rapid cooling. Since liquid nitrogen cannot provide an external oxygen supply to LSC, LSC-Q has lower oxygen content at room temperature compared to LSC-S. According to the principle of charge neutrality, the loss of oxygen leads to partial reduction of the variable-valent metal cations (Co^{n+}) and an increase in their ionic radii, resulting in lattice expansion in LSC.

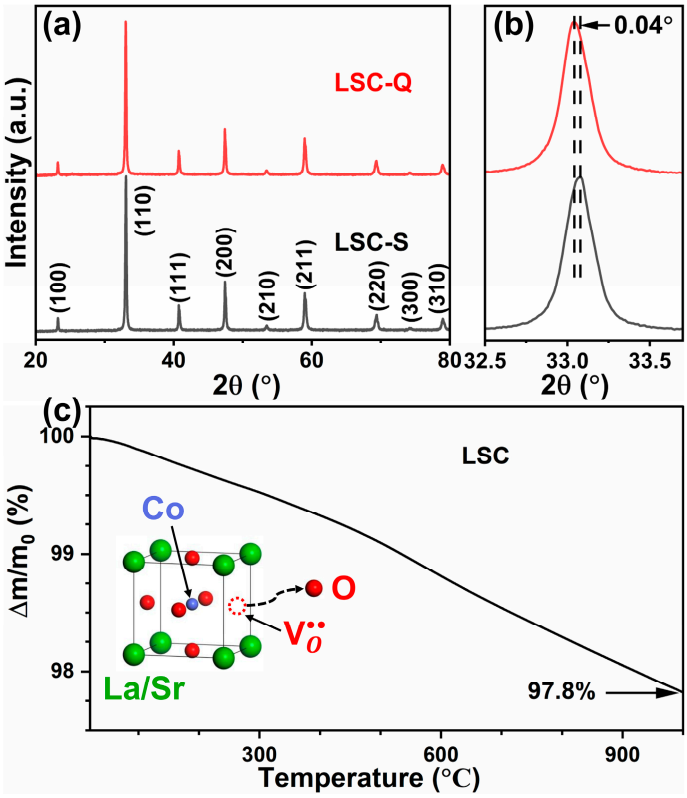


Figure 1. (**a**) The XRD patterns of the as-prepared LSC-S and LSC-Q and their (**b**) magnified images at the (110) crystal plane. (**c**) Mass change of LSC in an air atmosphere with temperature.

To examine the effect of the quenching process on the microstructure of LSC, the morphology of the cross-sections of bulk LSC-S and LSC-Q was observed using SEM. It is important to note that the cross-sections of the bulk were tested after the corresponding blocks were broken and left at room temperature in the air for 24 h. Figure 2a reveals that the cross-section of LSC-S is very smooth, and no segregation was observed, which is consistent with the observation of well-defined sharp surfaces in the TEM image (Figure S1a). Interestingly, a significant number of nano-segregated particles were observed in the cross-section of LSC-Q, as shown in Figure 2b. As shown in Figure S2, the surface of the freshly crushed LSC-Q is very smooth and no segregation particles can be observed. The comparison of morphology between Figures S2 and 2b indicates that the nanoparticles in Figure 2b were grown at room temperature.

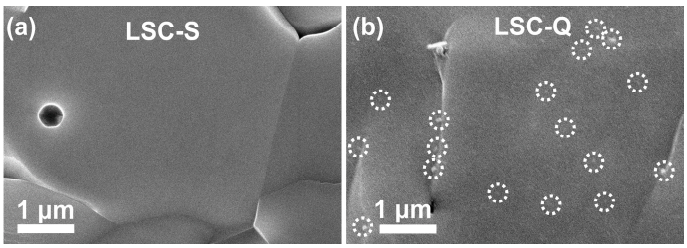


Figure 2. SEM images of (**a**) LSC-S and (**b**) LSC-Q cross-sections after being stored in air at room temperature for 24 h. The circles indicate segregated nanoparticles.

The TEM images of the corresponding LSC-Q bulk post ball milling and after 24 h of exposure to room temperature in air also revealed numerous nano-segregated particles (Figure 3a,b). The results in Figures 3c and S1b confirm that quenching can induce the segregation of components in LSC at room temperature in an air atmosphere, which is a very intriguing phenomenon. LSC is a typical perovskite-structured oxygen catalyst.

It is above 600 °C that $La_{0.6}Sr_{0.4}CoO_{3-\delta}$ exhibits the precipitation of cation components on the surface in the presence of air [12,24]. Common SOFC oxygen catalysts such as $La_{0.6}Sr_{0.4}Co_{0.2}Fe_{0.8}O_{3-\delta}$ [41] and $PrBaCo_2O_{5+\delta}$ [13] even have segregation temperatures of 400 °C and 700 °C, respectively. Component segregation at high temperatures not only leads to rapid performance deterioration but also poses a challenge to the removal of the inert layers. The ability to induce component segregation at room temperature provides a new avenue for controlling the performance of perovskite catalysts.

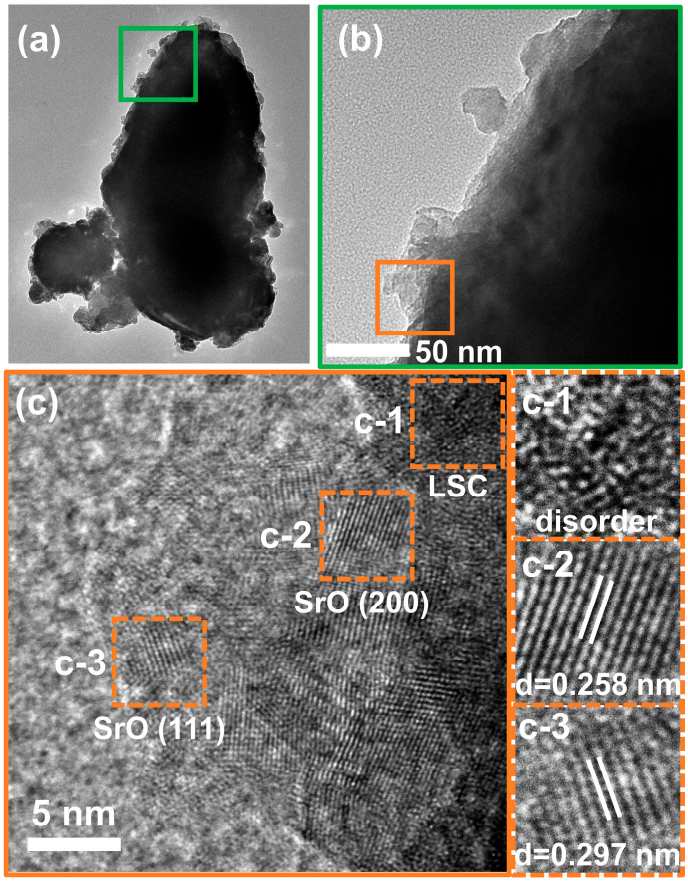


Figure 3. (**a**) TEM bright-field image of LSC-Q, and (**b**,**c**) its high-resolution TEM (HRTEM) images.

As observed in Figures 1b and 3c, the segregated particles display a nanocrystalline microstructure. The interplanar spacings, typically at 0.258 nm and 0.297 nm, align with the (200) and (111) planes of SrO. This suggests that the segregated metal cation in LSC is Sr, which can crystallize at room temperature. As shown in Figures 3c-1 and S1b-1, a large number of amorphous regions were found near the parent matrix of the segregated particles, providing useful clues to elucidate the underlying mechanism of Sr element segregation on the surface of LSC-Q at room temperature. As previous research has shown, the quenching process introduces a large number of lattice defects into the perovskite material lattice, such as disordered structures, point defects, and surface defects [30]. These defects are expected to significantly increase the lattice stress and electrostatic interaction forces in the perovskite matrix, providing it with enough "force" to drive the segregation of alkali earth metal Sr^{2+} to the surface at room temperature.

Before deploying LSC catalysts in SOFCs, high-temperature sintering is necessary to form the cathode layers. In our laboratory, the sintering temperature for SOFC cathode layers is 900 °C, with a holding time of 4 h. To investigate the physicochemical changes in the LSC cathode layers during the sintering process, the crystal structures of LSC-S and LSC-Q annealed at 900 °C for 4 h were characterized using the XRD technique. As shown in Figure 4a, both LSC-S and LSC-Q exhibit well-crystallized perovskite phases after

annealing. The difference in peak positions between the two samples is reduced from 0.04° before annealing to 0.02° after annealing, which may be closely related to factors such as the increased oxygen content in LSC-Q (Figure S4), Sr^{2+} segregation, and residual lattice defects [30]. Interestingly, after annealing, the content of high-valence Co ions (Co^{4+}) in LSC-Q is higher than in LSC-S (Figure 4c), which is closely related to factors such as the changing composition ratio and chemical defects in LSC. This result further confirms that the quenching process can indeed control the chemical environment of perovskite catalysts.

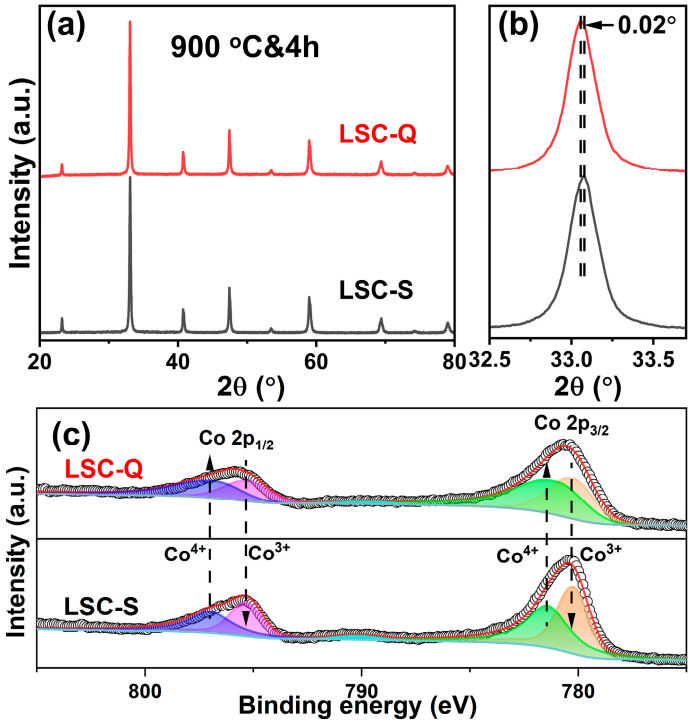


Figure 4. (**a**,**b**) XRD patterns of the LSC-S and LSC-Q annealed at 900 °C for 4 h and corresponding XPS spectra of (**c**) Co 2p.

To further reveal the evolution of the microstructure of LSC-S and LSC-Q during annealing, the two samples were analyzed using SEM and TEM techniques. As shown in Figure 5a, after annealing, LSC-S exhibits a small number of segregated particles on the surface. Figure 6a,b confirms that the segregated species in LSC-S have a nanocrystalline domain structure with an interplanar spacing of 0.297 nm, consistent with the (111) plane of SrO. It is worth noting that only a small number of SrO segregation particles of approximately 10 nm in size are formed in LSC-S after annealing at 900 °C for 4 h. In contrast, for LSC-Q, both the size and density of segregated particles after annealing at 900 °C for 4 h are significantly larger than those in LSC-S (Figures 5b and 6c,d), further confirming that the quenching process promotes the segregation of Sr^{2+} in LSC. As confirmed in Figure 6d, the segregated layer on the surface of LSC-Q, after annealing, maintains the nanocrystalline structure of SrO. Improving the cation conductivity of catalysts at room temperature is beneficial for the development of high-performance energy storage and conversion devices [42,43].

Figure 7a displays the area-specific resistance (ASR) values of symmetrical cells using LSC-S or LSC-Q electrodes, with GDC as the electrolyte across different temperatures. ASR is a crucial metric that reflects the catalytic activity of the catalyst for the oxygen reduction reaction. It can be seen from the figure that LSC-Q exhibits slightly higher ASR values compared to LSC-S, which is consistent with the conclusion that quenching can form more SrO inert segregation on the LSC surface (Figures 5 and 6). To further investigate the influence of the quenching process on the electrochemical performance of LSC catalysts, single cells based on LSC-S and LSC-Q were prepared using the same

process. Figure 7b shows the cross-sectional SEM image of a single cell based on the LSC-Q electrode, revealing a porous LSC-Q cathode layer, a thin GDC interlayer, a dense YSZ electrolyte layer, and a porous Ni-YSZ anode layer. The highest power density of the LSC-Q cathode at 800 and 750 °C, 0.95 and 0.72 W cm^{-2}, is slightly lower than the corresponding values for LSC-S (1.15 and 0.90 W cm^{-2} at 800 and 750 °C), suggesting that the aggregation of SrO segregation induced by quenching is not conducive to the improvement of the cell's electrochemical performance.

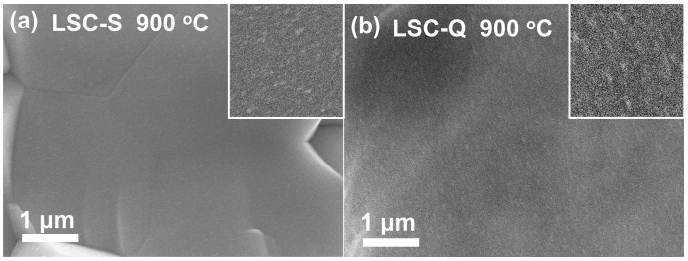


Figure 5. SEM images of (**a**) LSC-S and (**b**) LSC-Q after annealing at 900 °C for 4 h.

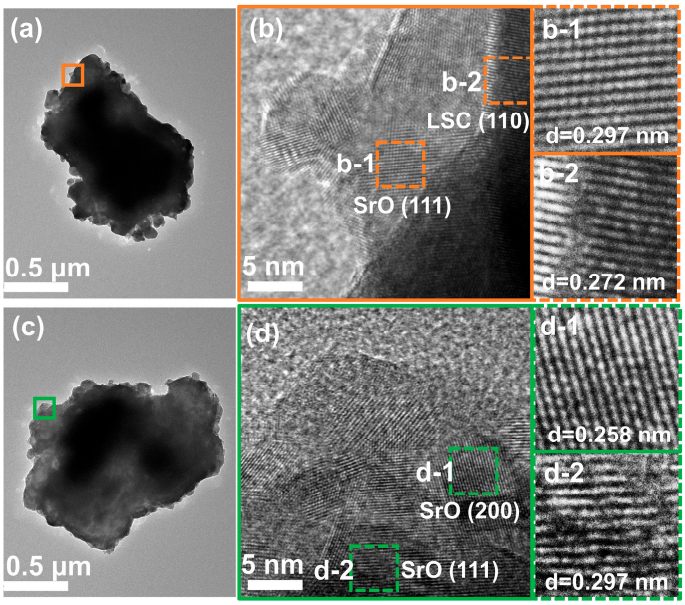


Figure 6. (**a**) BFTEM and (**b**) HRTEM images of LSC-S after annealing at 900 °C for 4 h. (**c**) BFTEM and (**d**) HRTEM images of LSC-Q after annealing at 900 °C for 4 h in air.

An intriguing observation, as depicted in Figure 7d, is the significant enhancement in the long-term stability of the LSC electrode attributable to the quenching process. For the single cell based on the LSC-S electrode, the output power density decreases steadily after 70 h. In contrast, there is no observed decline in the output power density of the single cell based on the LSC-Q electrode. This is likely due to the quenching process accelerating the segregation of Sr^{2+} in LSC, leading to an internal chemical environment that reaches an equilibrium and stable working state. Figure 7e presents the SEM image of the LSC-Q cathode after 110 h of discharge testing at 750 °C and 0.7 V. It can be seen that there are numerous segregation particles on the cathode surface, further confirming the view that the quenching process accelerates the segregation of Sr^{2+} in LSC, leading to an internal chemical environment in equilibrium and a stable working state.

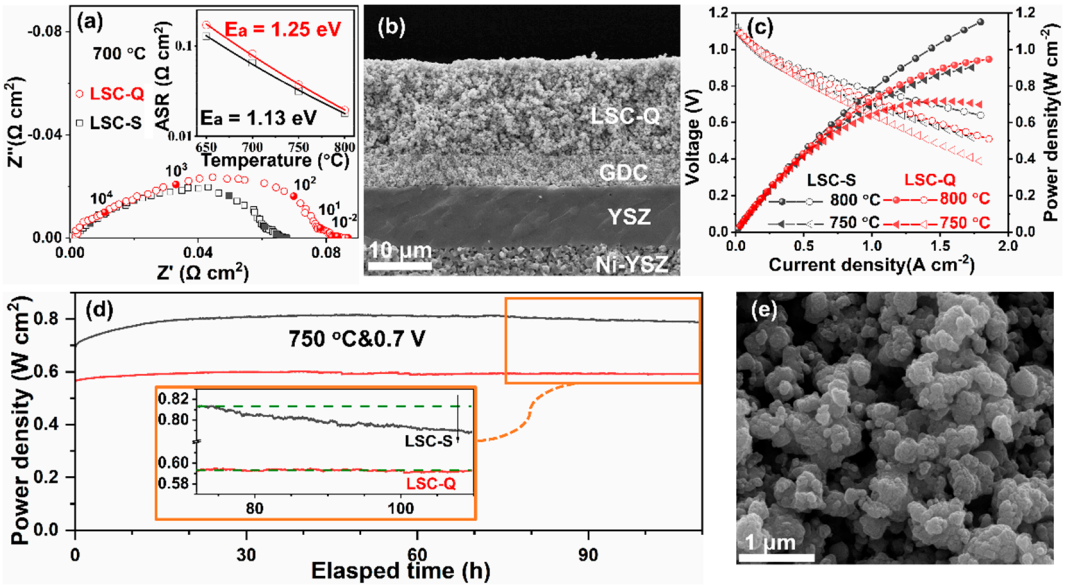


Figure 7. (**a**) Nyquist plots of symmetrical cells using LSC-S and LSC-Q as catalysts at 700 °C. The inset shows the ASR and activation energy at different temperatures. (**b**) cross-sectional SEM image of the SOFC single cell using LSC-Q as the electrode. (**c**) I-V-P and (**d**) P-t curves of SOFC single cells using LSC-S and LSC-Q as catalysts. (**e**) SEM morphology of the LSC-Q electrode after 110 h of single cell discharge testing at 750 °C and 0.7 V.

4. Conclusions

This work systematically investigates the impact of quenching on the microstructure and electrochemical behavior of LSC perovskite-structured oxygen catalysts. The quenching process described in this study involves rapidly transferring LSC bulk materials, at 1000 °C, into liquid nitrogen at approximately −200 °C, resulting in an actual cooling rate exceeding 400 °C s^{-1}. In contrast, the reference sample, denoted as LSC-S, follows the same fabrication process as LSC-Q except for the cooling process, which involves slow cooling in air at a rate of 0.05 °C s^{-1}. The research reveals that the quenching process does not alter the primary perovskite structure of LSC. However, during ambient storage in air, LSC-Q experiences in situ segregation of SrO nanoparticles. During the subsequent tempering process, more SrO segregation occurred than at room temperature. This phenomenon can be attributed to the quenching process, which introduces a substantial number of chemical defects into the perovskite matrix. These defects provide sufficient driving force for a partial migration of Sr^{2+} from the bulk to the particle surfaces, where they grow into SrO nanocrystalline domains. Symmetrical cell and single cell tests suggest that LSC-Q exhibits lower oxygen catalytic activity compared to LSC-S while showing superior long-term stability. This work presents a novel approach for inducing element segregation in perovskite catalysts at room temperature. It enriches the scientific understanding of oxygen catalysts and offers a new avenue for controlling the microstructure and electrochemical performance of perovskite catalysts under real operating conditions.

Supplementary Materials: The following supporting information can be downloaded at: https://www.mdpi.com/article/10.3390/coatings13122032/s1. Figure S1: HRTEM of (a) LSC-S and (b) LSC-Q; Figure S2: (a) SEM image of the freshly broken LSC-Q section and its (b) partially enlarged image; Figure S3: (a,b) TEM bright-field image of LSC-Q after being crushed into powder for 24 h; Figure S4: TGA of LSC-Q in air; Figure S5: Nyquist plots of LSC-S- and LSC-Q-based symmetrical cells at (a) 800 °C, (b) 750 °C, and (c) 650 °C; Figure S6: cross-section SEM image of the SOFC single cell based on an LSC-Q cathode; Figure S7: The (a) SEM image and mapping of (b) La, (c) Co, (d) Ce, (e) Zr, and (f) Ni elements of the LSC-Q-based SOFC cross-section.

Author Contributions: Conceptualization, S.P.; methodology, F.Z.; software, Y.Q.; validation, Y.Q.; formal analysis, F.Z.; investigation, F.Z.; resources, S.P.; data curation, F.Z.; writing—original draft preparation, F.Z.; writing—review and editing, S.P.; visualization, Y.Q.; supervision, S.P.; project administration, S.P.; funding acquisition, S.P. All authors have read and agreed to the published version of the manuscript.

Funding: This work was financially supported by the National Natural Science Foundation of China (Grant No. U2032157) and the Natural Science Foundation of Jiangsu Province (Grant No. BK20201425).

Institutional Review Board Statement: Not applicable.

Informed Consent Statement: Not applicable.

Data Availability Statement: The data presented in this study are available from the corresponding author upon request.

Conflicts of Interest: Fa Zheng was employed by the company Jiangsu Yushi Energy Group Co., Ltd. The remaining authors declare that the research was conducted in the absence of any commercial or financial relationships that could be construed as a potential conflict of interest.

References

1. Boldrin, P.; Brandon, N.P. Progress and outlook for solid oxide fuel cells for transportation applications. *Nat. Catal.* **2019**, *2*, 571–577. [CrossRef]
2. Pirou, S.; Talic, B.; Brodersen, K.; Hauch, A.; Frandsen, H.L.; Skafte, T.L.; Persson, Å.H.; Høgh, J.V.T.; Henriksen, H.; Navasa, M.; et al. Production of a monolithic fuel cell stack with high power density. *Nat. Commun.* **2022**, *13*, 1263. [CrossRef] [PubMed]
3. Ding, D.; Liu, M.F.; Liu, Z.B.; Li, X.X.; Blinn, K.; Zhu, X.B.; Liu, M.L. Efficient electro-catalysts for enhancing surface activity and stability of SOFC cathodes. *Adv. Energy Mater.* **2013**, *3*, 1149–1154. [CrossRef]
4. Li, Z.; Li, M.; Zhu, Z. Perovskite cathode materials for low-temperature solid oxide fuel cells: Fundamentals to optimization. *Electrochem. Energy Rev.* **2022**, *5*, 263–311. [CrossRef]
5. Zheng, F.; Pang, S. Progress in developing $LnBaCo_2O_{5+\delta}$ as an oxygen reduction catalyst for solid oxide fuel cells. *Catalysts* **2023**, *13*, 1288. [CrossRef]
6. Hanif, M.B.; Motola, M.; Qayyum, S.; Rauf, S.; Khalid, A.; Li, C.-J.; Li, C.-X. Recent advancements, doping strategies and the future perspective of perovskite-based solid oxide fuel cells for energy conversion. *Chem. Eng. J.* **2022**, *428*, 132603. [CrossRef]
7. Yatoo, M.A.; Habib, F.; Malik, A.H.; Qazi, M.J.; Ahmad, S.; Ganayee, M.A.; Ahmad, Z. Solid-oxide fuel cells: A critical review of materials for cell components. *MRS Commun.* **2023**, *13*, 378–384. [CrossRef]
8. Yatoo, M.A.; Skinner, S.J. Ruddlesden-Popper phase materials for solid oxide fuel cell cathodes: A short review. *Mater. Today Proc.* **2022**, *56*, 3747–3754. [CrossRef]
9. Pikalova, E.; Kolchugin, A.; Tsvinkinberg, V.; Sereda, V.; Khrustov, A.; Filonova, E. Comprehensive study of functional properties and electrochemical performance of layered lanthanum nickelate substituted with rare-earth elements. *J. Power Sources* **2023**, *581*, 233505. [CrossRef]
10. Li, L.; Kong, Z.; Yao, B.; Yang, H.; Gao, Z.; Xu, L.; Dong, F.; Ni, M.; Lin, Z. An efficient and durable perovskite electrocatalyst for oxygen reduction in solid oxide fuel cells. *Chem. Eng. J.* **2020**, *396*, 125237. [CrossRef]
11. Cai, C.; Xie, M.; Xue, K.; Shi, Y.; Li, S.; Liu, Y.; An, S.; Yang, H. Enhanced electrochemical performance of $La_{0.6}Sr_{0.4}Co_{0.2}Fe_{0.8}O_{3-\delta}$ cathode via Ba-doping for intermediate-temperature solid oxide fuel cells. *Nano Res.* **2022**, *15*, 3264–3272. [CrossRef]
12. Cai, Z.; Kubicek, M.; Fleig, J.; Yildiz, B. Chemical heterogeneities on $La_{0.6}Sr_{0.4}CoO_{3-\delta}$ thin films-correlations to cathode surface activity and stability. *Chem. Mater.* **2012**, *24*, 1116–1127. [CrossRef]
13. Pang, S.; Xu, J.; Su, Y.; Yang, G.; Zhu, M.; Cui, M.; Shen, X.; Chen, C. The role of A-site cation size mismatch in tune the catalytic activity and durability of double perovskite oxides. *Appl. Catal. B Environ.* **2020**, *270*, 118868. [CrossRef]
14. Koo, B.; Kim, K.; Kim, J.K.; Kwon, H.; Han, J.W.; Jung, W. Sr segregation in perovskite oxides: Why it happens and how it exists. *Joule* **2018**, *2*, 1476–1499. [CrossRef]
15. Feng, Z.; Hong, W.T.; Fong, D.D.; Lee, Y.L.; Yacoby, Y.; Morgan, D.; Shao-Horn, Y. Catalytic activity and stability of oxides: The role of near-surface atomic structures and compositions. *Acc. Chem. Res.* **2016**, *49*, 966–973. [CrossRef]
16. Wei, B.; Schroeder, M.; Martin, M. Surface cation segregation and chromium deposition on the double-perovskite oxide $PrBaCo_2O_{5+\delta}$. *ACS Appl. Mater. Interfaces* **2018**, *10*, 8621–8629. [CrossRef]
17. Chen, K.; Jiang, S.P. Surface segregation in solid oxide cell oxygen electrodes: Phenomena, mitigation strategies and electrochemical properties. *Electrochem. Energy Rev.* **2020**, *3*, 730–765. [CrossRef]
18. Cao, Y.; Gadre, M.J.; Ngo, A.T.; Adler, S.B.; Morgan, D.D. Factors controlling surface oxygen exchange in oxides. *Nat. Commun.* **2019**, *10*, 1346. [CrossRef]
19. Rupp, G.M.; Opitz, A.K.; Nenning, A.; Limbeck, A.; Fleig, J. Real-time impedance monitoring of oxygen reduction during surface modification of thin film cathodes. *Nat. Mater.* **2017**, *16*, 640–645. [CrossRef]

20. Kubicek, M.; Limbeck, A.; Frömling, T.; Hutter, H.; Fleig, J. Relationship between cation segregation and the electrochemical oxygen reduction kinetics of $La_{0.6}Sr_{0.4}CoO_{3-\delta}$ thin film electrodes. *J. Electrochem. Soc.* **2011**, *158*, B727–B734. [CrossRef]
21. Crumlin, E.J.; Mutoro, E.; Liu, Z.; Grass, M.E.; Biegalski, M.D.; Lee, Y.-L.; Morgan, D.; Christen, H.M.; Bluhm, H.; Shao-Horn, Y. Surface strontium enrichment on highly active perovskites for oxygen electrocatalysis in solid oxide fuel cells. *Energy Environ. Sci.* **2012**, *5*, 6081–6088. [CrossRef]
22. Feng, Z.; Crumlin, E.J.; Hong, W.T.; Lee, D.; Mutoro, E.; Biegalski, M.D.; Zhou, H.; Bluhm, H.; Christen, H.M.; Shao-Horn, Y. In situ studies of the temperature-dependent surface structure and chemistry of single-crystalline (001)-oriented $La_{0.8}Sr_{0.2}CoO_{3-\delta}$ perovskite thin films. *J. Phys. Chem. Lett.* **2013**, *4*, 1512–1518. [CrossRef]
23. Kubicek, M.; Rupp, G.M.; Huber, S.; Opitz, A.K.; Bernardi, J.; Stöger-Pollach, M.; Hutter, H.; Fleig, J. Cation diffusion in $La_{0.6}Sr_{0.4}CoO_{3-\delta}$ below 800 °C and its relevance for Sr segregation. *Phys. Chem. Chem. Phys.* **2014**, *16*, 2715–2726. [CrossRef] [PubMed]
24. Li, Y.; Zhang, W.; Wu, T.; Zheng, Y.; Chen, J.; Yu, B.; Zhu, J.; Liu, M. Segregation induced self-assembly of highly active perovskite for rapid oxygen reduction reaction. *Adv. Energy Mater.* **2018**, *8*, 1801893. [CrossRef]
25. Pang, S.; Song, Y.; Cui, M.; Tang, X.; Long, C.; Ke, L.; Yang, G.; Fang, T.; Guan, Y.; Chen, C. Rapid and durable oxygen reduction reaction enabled by a perovskite oxide with self-cleaning surface. *J. Energy Chem.* **2023**, *83*, 333–340. [CrossRef]
26. Li, Y.; Zhang, W.; Zheng, Y.; Chen, J.; Yu, B.; Chen, Y.; Liu, M. Controlling cation segregation in perovskite-based electrodes for high electro-catalytic activity and durability. *Chem. Soc. Rev.* **2017**, *46*, 6345–6378. [CrossRef] [PubMed]
27. Tsvetkov, N.; Lu, Q.; Sun, L.; Crumlin, E.J.; Yildiz, B. Improved chemical and electrochemical stability of perovskite oxides with less reducible cations at the surface. *Nat. Mater.* **2016**, *15*, 1010–1016. [CrossRef]
28. Pang, S.; Yang, G.; Jiang, X.; Shen, X.; Rao, D.; Chen, C. Insight into tuning the surface and bulk microstructure of perovskite catalyst through control of cation non-stoichiometry. *J. Catal.* **2020**, *381*, 408–414. [CrossRef]
29. Koo, B.; Kwon, H.; Kim, Y.; Seo, H.G.; Han, J.W.; Jung, W. Enhanced oxygen exchange of perovskite oxide surfaces through strain-driven chemical stabilization. *Energy Environ. Sci.* **2018**, *11*, 71–77. [CrossRef]
30. Ke, L.; Pang, S.; Long, C.; Fang, T.; Yang, G.; Song, Y.; He, X.; Ma, S.; Qian, Y.; Shen, X.; et al. Quenching-induced surface reconstruction of perovskite oxide for rapid and durable oxygen catalysis. *Chem. Eng. J.* **2023**, *463*, 142509. [CrossRef]
31. Fan, L.; Wang, J.; Huang, Z.; Yao, X.; Hou, N.; Gan, T.; Gan, J.; Zhao, Y.; Li, Y. Enhancement of the electrocatalytic activity of $La_{0.6}Sr_{0.4}Co_{0.2}Fe_{0.8}O_{3-\delta}$ through surface modification by acid etching. *Catal. Today* **2021**, *364*, 97–103. [CrossRef]
32. Siebenhofer, M.; Riedl, C.; Nenning, A.; Artner, W.; Rameshan, C.; Opitz, A.K.; Fleig, J.; Kubicek, M. Improving and degrading the oxygen exchange kinetics of $La_{0.6}Sr_{0.4}CoO_{3-\delta}$ by Sr decoration. *J. Mater. Chem. A* **2023**, *11*, 12827–12836. [CrossRef]
33. Choi, M.; Lee, W. Tuning the oxygen vacancy concentration in a heterostructured electrode for high chemical and electrochemical stabilities. *Chem. Eng. J.* **2022**, *431*, 134345. [CrossRef]
34. Li, J.; Zhou, X.; Wu, C.; Zhao, L.; Dong, B.; Wang, S.; Chi, B. Self-stabilized hybrid cathode for solid oxide fuel cell: A-site deficient perovskite coating as solid solution for strontium diffusion. *Chem. Eng. J.* **2022**, *438*, 135446. [CrossRef]
35. Zhou, M.; Liu, J.; Ye, Y.; Sun, X.; Chen, H.; Zhou, D.; Yin, Y.; Zhang, N.; Ling, Y.; Ciucci, F.; et al. Enhancing the intrinsic activity and stability of perovskite cobaltite at elevated temperature through surface stress. *Small* **2021**, *17*, 2104144. [CrossRef]
36. Lee, D.; Jacobs, R.; Jee, Y.; Seo, A.; Sohn, C.; Ievlev, A.V.; Ovchinnikova, O.S.; Huang, K.; Morgan, D.; Lee, H.N. Stretching epitaxial $La_{0.6}Sr_{0.4}CoO_{3-\delta}$ for fast oxygen reduction. *J. Phys. Chem. C* **2017**, *121*, 25651–25658. [CrossRef]
37. Kubicek, M.; Cai, Z.; Ma, W.; Yildiz, B.; Hutter, H.; Fleig, J. Tensile lattice strain accelerates oxygen surface exchange and diffusion in $La_{1-x}Sr_xCoO_{3-\delta}$ thin films. *ACS Nano* **2013**, *7*, 3276–3286. [CrossRef]
38. Zhuang, Z.; Li, Y.; Yu, R.; Xia, L.; Yang, J.; Lang, Z.; Zhu, J.; Huang, J.; Wang, J.; Wang, Y.; et al. Reversely trapping atoms from a perovskite surface for high-performance and durable fuel cell cathodes. *Nat. Catal.* **2022**, *5*, 300–310. [CrossRef]
39. Lee, W.; Han, J.W.; Chen, Y.; Cai, Z.; Yildiz, B. Cation size mismatch and charge interactions drive dopant segregation at the surfaces of manganite perovskites. *J. Am. Chem. Soc.* **2013**, *135*, 7909–7925. [CrossRef] [PubMed]
40. Pang, S.; Su, Y.; Yang, G.; Shen, X.; Zhu, M.; Wu, X.; Li, S.; Yang, X.; Xi, X. Enhanced electrochemical performance of Ca-doped $NdBa_{1-x}Ca_xCoCuO_{5+\delta}$ as cathode material for intermediate-temperature solid oxide fuel cells. *Ceram. Int.* **2018**, *44*, 21902–21907. [CrossRef]
41. Druce, J.; Téllez, H.; Burriel, M.; Sharp, M.D.; Fawcett, L.J.; Cook, S.N.; McPhail, D.S.; Ishihara, T.; Brongersma, H.H.; Kilner, J.A. Surface termination and subsurface restructuring of perovskite-based solid oxide electrode materials. *Energy Environ. Sci.* **2014**, *7*, 3593–3599. [CrossRef]
42. Li, W.; Chu, X.-S.; Wang, F.; Dang, Y.-Y.; Liu, X.-Y.; Wang, X.-C.; Wang, C.-Y. Enhanced cocatalyst-support interaction and promoted electron transfer of 3D porous g-C_3N_4/GO-M (Au, Pd, Pt) composite catalysts for hydrogen evolution. *Appl. Catal. B Environ.* **2021**, *288*, 120034. [CrossRef]
43. Wang, M.; Jiang, C.; Zhang, S.; Song, X.; Tang, Y.; Cheng, H.-M. Reversible calcium alloying enables a practical room-temperature rechargeable calcium-ion battery with a high discharge voltage. *Nat. Chem.* **2018**, *10*, 667–672. [CrossRef]

Disclaimer/Publisher's Note: The statements, opinions and data contained in all publications are solely those of the individual author(s) and contributor(s) and not of MDPI and/or the editor(s). MDPI and/or the editor(s) disclaim responsibility for any injury to people or property resulting from any ideas, methods, instructions or products referred to in the content.